Characterization of the mechanical properties of the mouse Achilles tendon enthesis by microindentation. Effects of unloading and subsequent reloading

Claire Camy [a], Tilman Grünewald [b], Edouard Lamy [a], Flavy Roseren [a,c], Mathieu Caumes [a], Théo Fovet [d], Thomas Brioche [d], Cecile Genovesio [e], Angèle Chopard [d], Martine Pithioux [a,c,f,1], Sandrine Roffino [a,*,1]

[a] *Aix Marseille Univ, CNRS, ISM, 13009 Marseille, France*
[b] *Aix Marseille Univ, CNRS, Centrale Marseille, Institut Fresnel, Marseille, France*
[c] *Aix Marseille Univ, APHM, CNRS, ISM, Mecabio Platform, Department of Orthopaedics and Traumatology, 13009 Marseille, France*
[d] *DMEM, Montpellier University, INRAE, UMR 866, Montpellier, France*
[e] *Aix Marseille Univ, Faculté de Pharmacie, Marseille, France*
[f] *Aix Marseille Univ, APHM, CNRS, ISM, Sainte-Marguerite Hospital, Institute for Locomotion, Department of Orthopaedics and Traumatology, 13009 Marseille, France*

ARTICLE INFO

ABSTRACT

The fibrocartilaginous tendon enthesis, i.e. the site where a tendon is attached to bone through a fibrocartilaginous tissue, is considered as a functionally graded interface. However, at local scale, a very limited number of studies have characterized micromechanical properties of this transitional tissue. The first goal of this work was to characterize the micromechanical properties of the mineralized part of the healthy Achilles tendon enthesis (ATE) through microindentation testing and to assess the degree of mineralization and of carbonation of mineral crystals by Raman spectroscopy. Since little is known about enthesis biological plasticity, our second objective was to examine the effects of unloading and reloading, using a mouse hindlimb-unloading model, on both the micromechanical properties and the mineral phase of the ATE. Elastic modulus, hardness, degree of mineralization, and degree of carbonation were assessed after 14 days of hindlimb suspension and again after a subsequent 6 days of reloading. The elastic modulus gradually increased along the mineralized part of the ATE from the tidemark to the subchondral bone, with the same trend being found for hardness. Whereas the degree of carbonation did not differ according to zone of measurement, the degree of mineralization increased by >70 % from tidemark to subchondral bone. Thus, the gradient in micromechanical properties is in part explained by a mineralization gradient. A 14-day unloading period did not appear to affect the gradient of micromechanical properties of the ATE, nor the degree of mineralization or carbonation. However, contrary to a short period of unloading, early return to normal mechanical load reduced the micromechanical properties gradient, regardless of carbonate-to-phosphate ratios, likely due to the more homogeneous degree of mineralization. These findings provide valuable data not only for tissue bioengineering, but also for musculoskeletal clinical studies and microgravity studies focusing on long-term space travel by astronauts.

1. Introduction

The musculoskeletal system provides our body with movement. Tendons play a major role in bone segment mobility, transmitting muscle force to the bone through two interfaces: the myotendinous junction and the osteotendinous junction (Curzi, 2016; Roffino et al., 2021). The latter, also called enthesis, is responsible for force transmission between two tissues with differing mechanical properties: the tendon (soft tissue) and the bone (hard tissue). When tendons insert into the long bone epiphysis, as with the Achilles tendon, the entheses are

---

fibrocartilaginous; i.e. approaching the bone, the tendon progressively differentiates into a fibrocartilaginous tissue whose distal part adjacent to the bone is calcified.

The gradual transition from tendon fibrous tissue to enthesis fibrocartilage has been described at different scales. First, the molecular composition of the different collagens and proteoglycans varies from the tendon to the subchondral interface. The fibrous zone of the enthesis is rich in collagen I and III and small leucin-rich proteoglycans (SLRPs) (Roffino et al., 2021). These molecules were also described in the uncalcified entheseal fibrocartilage (Roffino et al., 2021; Thomopoulos et al., 2003; Waghray et al., 2015; Waggett et al., 1998). However, the latter is additionally composed of type II collagen and aggrecan, two macromolecules typical of fibrocartilaginous tissue (Camy et al., 2022; Friese et al., 2020; Moriggl et al., 2003). These molecules are also present in the calcified part of the entheseal fibrocartilage (CFc), where the extracellular matrix specifically expresses collagen X (Cury et al., 2016; Shaw and Benjamin, 2007; Thomopoulos et al., 2003) and has a mineral phase. Using Raman spectroscopy, the mineral's smooth transition between fibrocartilage and bone was demonstrated (Wopenka et al., 2008; Genin et al., 2009) by a reported gradation in the mineral-to-collagen ratio from tendon to bone in the functional supraspinatus tendon enthesis. In addition to the molecular composition of the enthesis, a gradient exists in the organization and the distribution of the tissue components. As the collagen fibers approach the bone, there is a progressive decrease both in their cross-sectional area (Sartori and Stark, 2020) and in their degree of alignment along the tendon-to-bone insertion (Genin et al., 2009; Sartori and Stark, 2020), modifying their organization relative to the tendon fibers (Thomopoulos et al., 2003). Moreover, the distribution of mineral crystals is documented as dependent on their position relative to the ossification front (tidemark), unlike bioapatite crystal size. While the gradient starts with the minerals predominantly located outside the collagen fibrils near the tidemark, they appear intrafibrillar and extrafibrillar at the end of the gradient close to the bone (Deymier et al., 2019). Finally, from a cellular point of view, changes in the shape and size of the cells along the longitudinal axis of the enthesis were described, strongly suggesting a gradual cell phenotype (Thomopoulos et al., 2003; Zhang et al., 2022). The fibroblasts of the fibrous zone are gradually replaced by fibrochondrocytes aligned with the direction of principal force (Roffino et al., 2021; Tits et al., 2021; Zhang et al., 2022) and gradually increase in size from the tendon to the osteochondral interface (Zhang et al., 2022). Round in shape in the unmineralized fibrocartilage, the fibrocartilage cells are more elongated in the CFc and embedded in the mineralized matrix (Kumagai et al., 1994; Ralphs et al., 1992).

These compositional, cellular, and organizational gradients along the longitudinal axis of the enthesis led some authors to consider fibrocartilaginous entheses as a functionally graded interface (Schwartz et al., 2012; Smith et al., 2012) protecting the structure from risk of failure during force transmission (Liu et al., 2011; Shaw and Benjamin, 2007; Zelzer et al., 2014) by locally mitigating stress concentrations (Bunker et al., 2014; Smith et al., 2012). This concept of a functional gradient assumes that the biological gradients lead to gradual mechanical properties transition between soft tendon and hard bone. While this mechanical gradient was predicted by mathematical models concerning the attachment of tendon to bone (Genin et al., 2009; Thomopoulos et al., 2003), a recent experimental study did not reveal any gradient in the local micromechanical properties of the Achilles tendon enthesis in rats (Tits et al., 2023). This unexpected experimental result calls for further investigation, in view of the challenge of developing novel biomimetic therapeutic strategies for enthesis regeneration.

The first goal of our work was thus to characterize, through microindentation testing, the micromechanical properties along the longitudinal axis of the mineralized part of the healthy Achilles tendon enthesis (ATE) in mice. As some authors hypothesized an uneven distribution of the mechanical stresses applied to the ATE, with force transmission actually occurring in the superficial part of the enthesis (Benjamin and McGonagle, 2001), we also examined the micromechanical properties along the anteroposterior axis. Because the local mechanical properties of the enthesis are dependent on the mineral phase of the extracellular matrix (Deymier et al., 2017; Golman et al., 2021), we investigated the degree of mineralization and of carbonation of mineral crystals by Raman spectroscopy as a source of possible variations in micromechanical properties.

Previous studies described an enthesis tissue remodeling in response to chronic variations in mechanical load (Roffino et al., 2021; Kannus et al., 1996; Järvinen et al., 1999; Deymier et al., 2019; Abraham et al., n.d.; Mutsuzaki et al., 2015; Deymier et al., 2020; Frizziero et al., 2011; Camy et al., 2022). Thus, a second objective of our study was to examine the effects of an altered mechanical environment on both the micromechanical properties and the mineral phase of the Achilles tendon enthesis. We chose to unload the mouse ATE using a hindlimb-unloading model, commonly used to simulate weightlessness (Morey-Holton and Globus, 1998). Mice were hindlimb-suspended for two weeks. The same parameters were assessed on mice reloaded for 6 days following the unloading period to study the effects of the return to normal mechanical stress.

2. Materials and methods

2.1. Animals and experimental procedure

Thirty 12-week-old male C57BLACK6J mice (24.84 g $\pm$ 1.26) were used for this study, approved by the Committee on the Ethics of Animal Experiments of Languedoc Roussillon in accordance with the guidelines from the French National Research Council for the Care and Use of Laboratory Animals (APAFIS#28764-2020122115407491). Mice were housed in single cages in temperature-controlled rooms (22 °C) under a 12 h light-dark cycle and were fed a standard diet ad libitum. Maximum care was taken to minimize animal discomfort and suffering.

Ten mice moved freely in their cages throughout the experiment, constituting the Control (CTL) condition. Twenty other mice were hindlimb-unloaded through tail suspension for 14 days to simulate weightlessness according to the Morey-Holton and Globus (1998) procedure previously described (Amblard et al., 2003; Camy et al., 2022). Following suspension, ten mice were euthanized; this constitutes the Hindlimb Unloaded (HU) condition. For the remaining ten mice, ambulation recovery was allowed for six days before euthanization; this constitutes the Hindlimb Unloaded and Reloaded (HUR) condition. The following experiments were performed on the right hindlimb of each animal.

2.2. Microindentation testing

2.2.1. Block preparation

Six ankles per condition (CTL, HU, HUR), including the tibio-talus and the talo-calcaneal joints, were dissected and prepared for resin embedding as previously described (Camy et al., 2022; Roseren et al., 2022). The samples were fixed in 4 % paraformaldehyde (Merk Millipore) in 0.01 M pH 7.4 phosphate buffer saline (Sigma-Aldrich) for 1 week before being dehydrated in progressively increasing concentrations of ethanol, remaining in each for 48 h. The samples were then soaked in methylcyclohexane (VWR international) for 2 days. Finally, the ankles were embedded in methylmetacrylate (VWR international). The resin blocks were polymerized at 28 °C.

The specimens were cut sagittally up to the median part of the enthesis with a microtome (Leica RM 2265, Wetzlar, Germany) using a D-profile tungsten-carbide knife. The blocks were polished with an ESC-200-GTL polishing machine (ESCIL, Chassieu, France) to provide a uniform surface and to remove any residual resin on the sample. They were first polished with carbide paper (PFA G2500, ESCIL, Chassieu, France) for 1 min, followed by thinner polishing with satin polishing discs (MAGNET, ESCIL, Chassieu, France) coupled with 6 μm, 3 μm, 1

μm and 0.25 μm polycrystalline diamond slurries (ECN poly, ESCIL, Chassieu, France) respectively for 3 min each. Between diamond slurries, the blocks were cleaned in an ultrasonic distilled water bath to remove any residuals.

2.2.2. Microindentation procedure

Microindentation testing was performed on the CFc with an NHT[2] device (Anton Paar, Graz, Austria) equipped with a diamond Berkovitch-type indenter, base length 120 nm (Elastic modulus: 1141 GPa; Poisson's ratio: 0.07). The CFc was divided into four zones in the proximo-distal axis from the tidemark to the CFc-bone interface, with one zone added on the subchondral bone near the interface, using an average of five indents per zone (Fig. 1A). The CFc was also divided into two regions according to the antero-posterior axis: a deep region, D (anterior region of the enthesis) and a superficial region, S (posterior region of the enthesis) (Fig. 1A). In the HUR enthesis, a neomineralization area had formed in response to reloading in the superficial part of the enthesis (Camy et al., 2022), so an extra zone 0 was added to these samples for the analysis. The indents were performed along the collagen fibers located between the rows of fibrochondrocytes, avoiding microporosity caused by the cells. In order to determine (pre-indentation) and to verify (post-indentation) the location of the indents, 5-μm thick histological sections were collected before polishing and after microindentation testing. Sections were stained with toluidine blue and Von Kossa following the procedure previously described (Camy et al., 2022) (Fig. 2).

The microindentation experiment was performed based on a trapezoidal load profile. The experiment comprised a loading phase to reach 25 mN at 50 mN/min, a 30-s holding phase at 25 mN, and an unloading phase to return to 0 N at 50 mN/min. The experiments were performed at a controlled temperature of 22 °C. The average penetration depth of an indent being around 1.6 μm, a 20 μm distance was left between indents. Moreover, we inspected post-indentation surfaces of one random sample using scanning electron microscopy to ensure the absence of microcracks due to sample preparation.

Elastic modulus E_s and hardness H were calculated according to the Oliver and Pharr method (Oliver and Pharr, 1992). Elastic modulus E_s was calculated according to the following equation:

$$E_s = \frac{(1 - \vartheta_s^2)}{\left(\frac{1}{E_r} - \frac{(1 - \vartheta_i^2)}{E_i}\right)} \tag{1}$$

ν_s is the Poisson's ratio of the material fixed at 0.3, this value being applied to indentation testing both on bone (Turner and Burr, 2001) and on fibrocartilage (Hu et al., 2001). E_i and ν_i respectively represent the elastic modulus and Poisson's ratio of the indenter and E_r is the reduced modulus calculated according to equation:

$$E_r = \frac{\sqrt{\pi}}{2} \frac{S}{\sqrt{A_c}} \tag{2}$$

with S representing the unloading stiffness and A_c representing the contact area between the indenter and the sample. Finally, hardness was calculated according to the equation:

$$H = \frac{P_{max}}{A_c} \tag{3}$$

with P_{max} the maximum load.

Prior to testing, the indentation protocol was tested on a silica block of known elastic modulus (72 GPa) and Poisson's ratio (0.17) in order to calibrate the device. In addition, the elastic modulus and hardness of the embedding resin were characterized. Any sample values too similar to those of the resin (E_s = 3.963 (± 0.127) GPa; H = 0.171 (±0.011) GPa) were excluded from the analysis.

2.3. Raman spectroscopy

Four ankles per condition (CTL, HU, HUR) were dissected according to the same protocol as for the indentation study. Samples were embedded in tissue-freezing medium (Leica) and cryofixed at −80 °C for slow freezing. Fourteen-μm-thick sections of undecalcified samples were
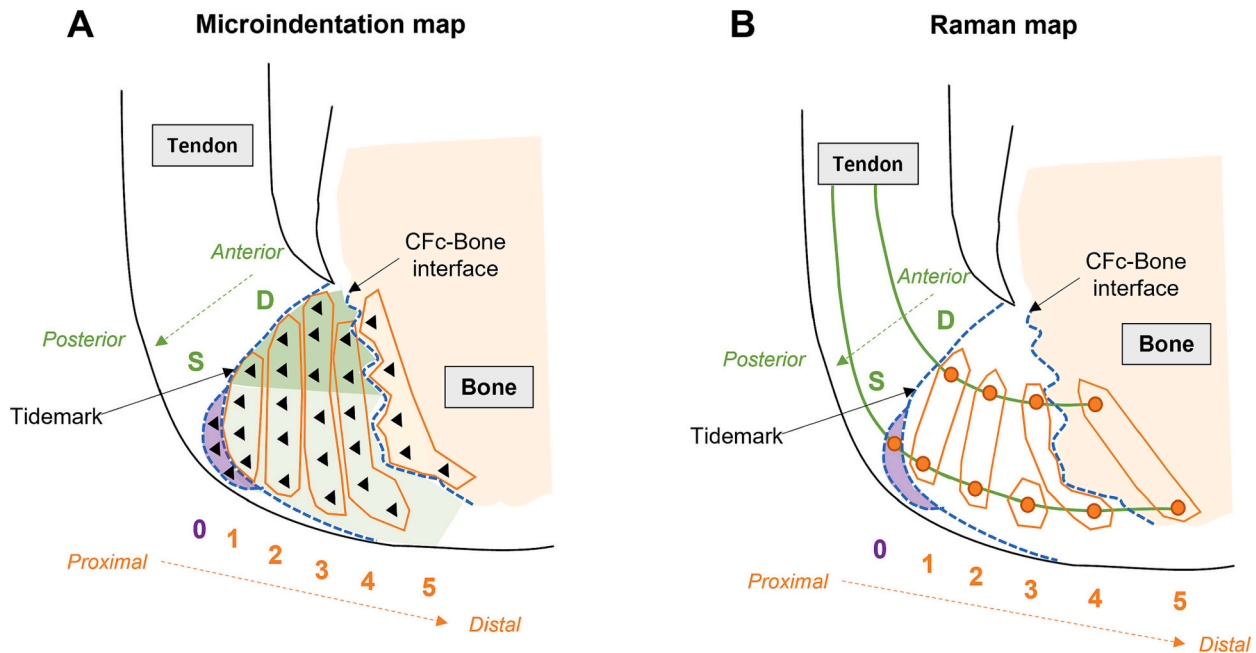

Fig. 1. Mapping of the experiments. A: Indentation map. The enthesis was divided into five zones from the tidemark to the subchondral bone in the proximo-distal axis (orange) and the CFc was divided into two regions, deep (D) and superficial (S), in the antero-posterior axis (green). B: Raman map. Two lines of spectra were acquired: one in the deep (D) and one in the superficial (S) regions of the enthesis by following collagen fibers (green line). These two lines were divided into 4 or 5 zones, including one in the subchondral bone for the D and the S regions, respectively. For each experiment, a zone Z0 on the superficial part of the CFc was added for the HUR samples (purple area), corresponding to the newly-mineralized zone we previously observed in response to reloading (Camy et al., 2022).
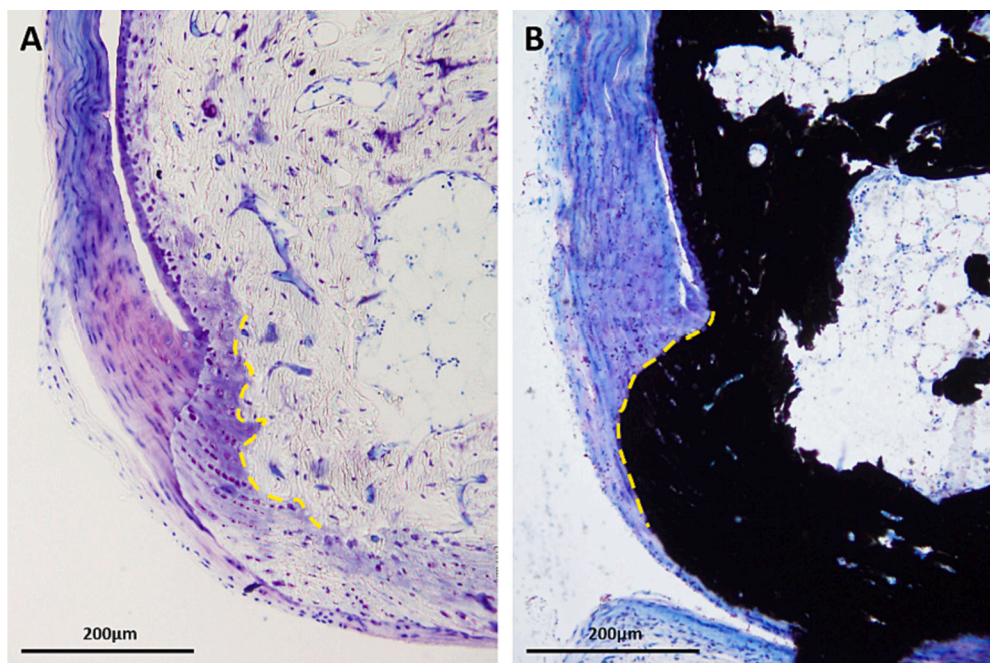
Fig. 2. An example of histological sections of enthesis used for the mapping. A: Toluidine blue staining, highlighting the CFc-bone interface (yellow dashed line). B: Von Kossa staining, highlighting the mineralization front (yellow dashed line).

obtained using a cryostat (Leica© CM3050S, Wetzlar, Germany) and placed onto Superfrost Plus slides.

Prior to Raman spectroscopy, the sections were defrosted and rehydrated in distilled water to remove the embedding medium. To determine the location of the enthesis, the mineralization front and the CFc-bone interface were visualized with a polarized light microscope (Nikon Eclipse LV1000 N POL, Tokyo, Japan) before the experiment. Raman spectra were acquired using a Raman spectrometer (Horiba LabRam HR, Kyoto, Japan) in reflection mode equipped with a $100\times$ air objective (Olympus MPlan, NA 0.9), a Peltier-cooled CCD camera, and a laser excitation wavelength of 632.8 nm. The power delivered to the sample

was about 1 mW. The spectrometer was calibrated using an Si standard prior to every experiment. A 600 lines/mm grating was used, giving access to a spectral window ranging from 600 to 1800 cm^{-1}. For each point, a 30-s acquisition time with 10 repetitions was chosen. The potential effects of polarized Raman spectroscopy highlighted by Kazanci et al. (2006) on human cortical lamellar bone were investigated in our region of interest. We determined the amide I/amide III ratios for each zone in each experimental condition, and statistical analysis showed no significant effect of polarization due to the large probed volume assessed (data not shown).

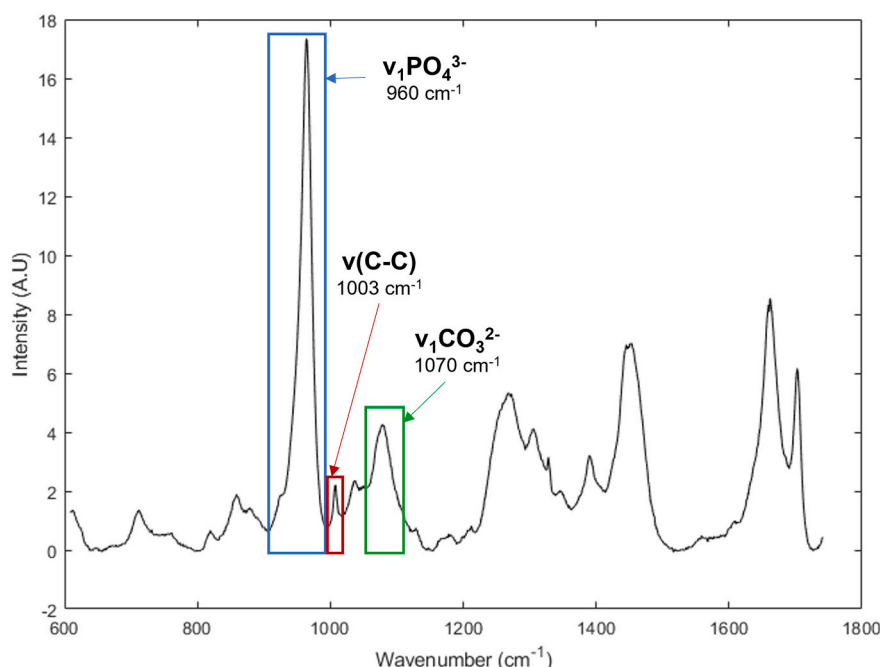Each spectrum was processed using home-written MATLAB code.

Fig. 3. Raman spectra acquisition. Ratios take into account peaks of phosphate (blue rectangle), phenylalanine (red rectangle), and carbonate (green rectangle).

First, a fifth-order polynomial was fitted with an asymmetric truncated quadratic cost function to remove the background over the whole spectral range (Mazet et al., 2005). Three peaks were selected for further investigation (Fig. 3): the $\nu_1 PO_4^{3-}$ peak at 960 cm^{-1} for phosphate apatite, the ν(C—C) phenylalanine peak at 1003 cm^{-1} for collagen, and the $\nu_1 CO_3^{2-}$ peak at 1070 cm^{-1} for carbonate apatite (Das Gupta et al., 2020; Mandair and Morris, 2015). From the maximum peak intensities, two intensity ratios were determined: the mineral-to-matrix ratio, that between the phosphate peak and the phenylalanine peak, and the carbonate-to-phosphate ratio, which indicates the proportion of carbonate-substituted phosphate apatites (Crawford-Manning et al., 2021; Deymier et al., 2020; Schwartz et al., 2013; Mandair and Morris, 2015).

Similar to the microindentation experiment, the D and S regions of the CFc were investigated (Fig. 1B). In each of these areas, Raman spectra were acquired at several points uniformly distributed between the tidemark and the subchondral bone, taking care to respect the orientation of collagen fibers. In this way, zones 1 to 5 were determined along the proximo-distal axis (Fig. 1B). In addition, a zone 0 was added at the superficial line of the HUR samples, to investigate the newly-formed mineralized fibrocartilage. For each condition (CTL, HU, HUR), spectra were collected on two sections per sample. Due to loss of one sample during the sectioning process, only three out of four CTL samples were tested.

2.4. Statistical analysis

First, a 2-way mixed ANOVA was performed using RStudio software to assess the effects of condition (CTL, HU, HUR) and zone (0 to 5) on elastic modulus, hardness, mineral-to-matrix ratio, and carbonate-to-phosphate ratio. Another 2-way mixed ANOVA was performed to assess the effects of condition and region (D and S) on the same data, but only on the CFc. Before each test, the normality of data, the homogeneity of variances, and the sphericity of intra-individual covariances were verified. When there was significant interaction between two variables or to investigate the main effect, pairwise *t*-tests with Bonferroni correction were performed post-hoc to compare the data pairwise, with significance level set at $p = 0.05$.

3. Results

3.1. Micromechanical properties of the Achilles tendon enthesis

3.1.1. Micromechanical properties along the longitudinal axis of the enthesis

Two-way mixed ANOVA models were used to compare elastic moduli and hardness in the different conditions (CTL, HU, HUR) according to the zone where the indents were performed. On elastic modulus, statistical analysis showed a significant effect of zone ($p < 0.0001$), no effect of condition, and an interaction between the two factors ($p = 0.026$). In the CTL samples (Fig. 4A), the elastic modulus increased from 6.97 GPa (± 1.03) to 12.88 GPa (±1.70) from the tidemark (Z1) up to the subchondral bone (Z5). In the CFc, the elastic moduli of zones 1, 2, and 3 were significantly lower than that at the CFc-bone interface (Z4) ($p = 0.0008$ for Z1, $p = 0.008$ for Z2, and $p = 0.002$ for Z3). They were also lower than the elastic modulus in the subchondral bone (Z5) ($p = 0.015$ for Z1, $p = 0.043$ for Z2, and $p = 0.034$ for Z3). The HU samples (Fig. 4B) showed similar behavior to the CTL samples, with a gradual increase in elastic modulus from the tidemark (6.96 GPa ± 1.12) to the bone (13.25 GPa ± 1.22). Both the Z1 and Z2 elastic moduli were significantly lower than the Z4 and Z5 elastic moduli ($p = 0.0006$ and $p < 0.0001$ for Z1 and $p = 0.001$, and p = 0.0008 for Z2). In the HUR samples (Fig. 4C) with an additional zone Z0 indented (Fig. 1), no significant difference was found between the different CFc zones. We only observed a significant difference in elastic modulus between the subchondral bone (Z5) and all CFc zones (0, 1, 2, 3, and 4), with the elastic moduli of all CFc zones significantly lower than that of the bone ($p = 0.017$ for Z0, $p = 0.008$ for Z1, $p = 0.014$ for Z2, $p = 0.003$ for Z3, and $p = 0.013$ for Z4). Finally, we found that the HUR samples had a significantly lower elastic modulus than the CTL samples at the CFc-bone interface (Z4) ($p = 0.013$).

Based on the two-way mixed ANOVA model, hardness appeared to be significantly dependant on the zone ($p < 0.0001$) but not on the condition. In addition, there was an interaction between zone and condition ($p = 0.035$). The hardness of the CTL samples (Fig. 4D) increased by 60 % from Z1 (0.290 GPa ± 0.05) to Z5 (0.465 GPa ± 0.11), not statistically significant due to the large dispersion of the data. However, within the CFc, the hardness values of Z1 and Z3 were significantly lower than those of Z4 ($p = 0.022$ for Z1 and $p = 0.015$ for Z3). No significant
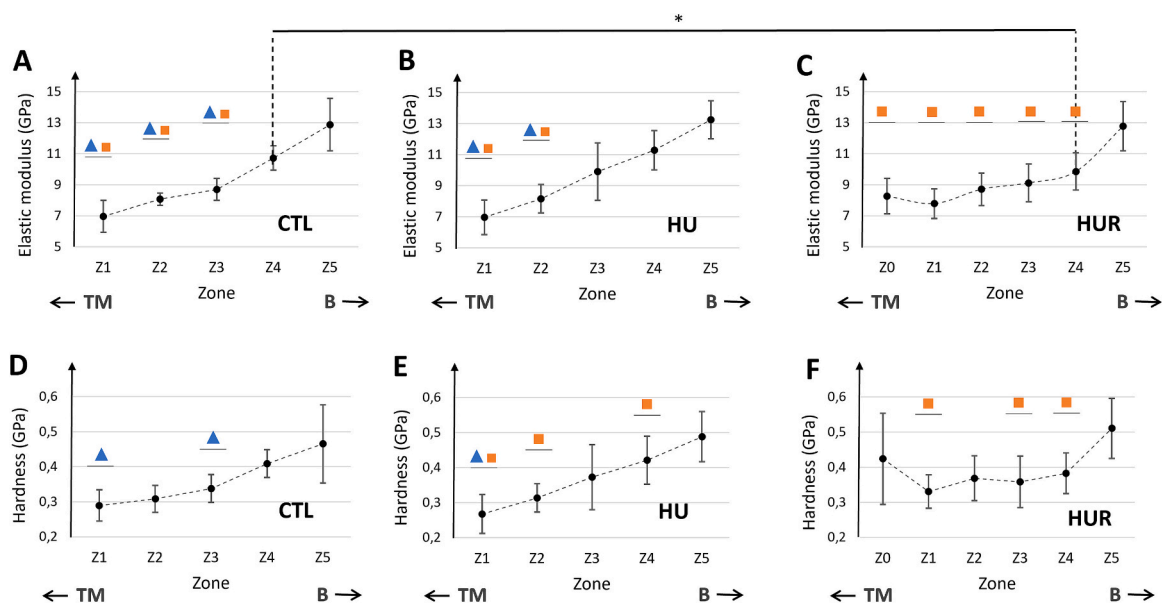

Fig. 4. Elastic modulus (A, B, C) and Hardness (D, E, F) according to ATE zone in CTL (A, D), HU (B, E) and HUR (C, F) conditions. Z1, Z2, Z3, and Z4 are the CFc zones, with Z1 and Z4 respectively the most proximal and the most distal to the tidemark. Z5 is the subchondral bone zone. TM: Tidemark. B: Bone. Blue triangle ▲: significantly different from Z4 ($p < 0.05$). Orange square ■: significantly different from Z5 ($p < 0.05$). *: significant difference between conditions (p < 0.05).

difference was observed between the CFc zones (1–4, and) and the subchondral bone (Z5). The HU samples (Fig. 4E) exhibited the same behavior as the CTL samples, with hardness increasing in the same way from Z1 (0.268 GPa ± 0.06) to Z5 (0.489 GPa ± 0.07). Inside the CFcs, the hardness near the tidemark (Z1) was significantly lower than the hardness near the CFc-bone interface (Z4) ($p = 0.002$). The subchondral bone (Z5) was also significantly harder than zones 1, 2, and 4 of the CFc ($p < 0.0001$ for Z1, p = 0.015 for Z2, and $p = 0.026$ for Z4). For the HUR samples (Fig. 4F), no significant difference in hardness was found between the different zones of the CFc, including Z0. Only the subchondral bone (Z5) was significantly harder than zones 1, 3, and 4 ($p = 0.006$ for Z1, $p = 0.003$ for Z3, and $p = 0.016$ for Z4). Finally, no zone showed any significant difference in hardness according to condition.

3.1.2. Micromechanical properties along the antero-posterior axis of the enthesis

A second set of two-way mixed ANOVA was used to compare elastic moduli and hardness in the different conditions (CTL, HU, HUR) according to CFc region. Contrary to zone, we did not find statistically significant interactions between region and condition, despite a significant effect of region ($p = 0.012$). The latter showed that, regardless of condition and zone, elastic modulus values were higher in the deep region of the CFc than in the superficial region. To investigate whether this effect prevailed in each condition, we compared the elastic moduli of the deep and superficial regions of the CFcs for each condition and observed no significant difference in any condition (Fig. 5A-C). Finally, neither condition nor region had an effect on the hardness of the CFcs (Fig. 5D-F).

3.2. Raman spectroscopy experiment results

Concerning the distribution of the phosphate-to-collagen ratio along the longitudinal axis of the ATE, statistical analysis highlighted a significant effect of zone ($p < 0.0001$) but no effect of condition (Fig. 6) and no significant interaction between zone and condition. We investigated whether the zone effect applied to each condition. On the CTL samples (Fig. 6A), the phosphate-to-collagen ratio increased from 14.80 (±2.41) at the tidemark (Z1) to 25.49 (±3.35) in the subchondral bone (Z5). Statistically, only the Z2 phosphate-to-collagen ratio differed from the

subchondral bone ratio ($p = 0.048$). The HU condition showed the same pattern of ratio variation along the longitudinal axis of the enthesis, with the phosphate-to-collagen ratio increasing from 14.76 (±1.71) at the tidemark (Z1) to 21.66 (±5.40) in the subchondral bone (Z5) (Fig. 6B). HU condition Z1 and Z2 ratios were significantly lower than the phosphate-to-collagen ratio of the subchondral bone (Z5) ($p = 0.042$ for Z1 and p = 0.048 for Z2). Finally, in the HUR condition, where an additional zone Z0 was investigated (Fig. 1), no significant difference was observed between the different zones. However, despite a high standard deviation in HUR, the phosphate-to-collagen ratio of the subchondral bone (Z5) seemed to be higher than for CFc, where the phosphate-to-collagen ratios were homogenous (Fig. 6C). In contrast to the phosphate-to-collagen ratio, neither zone nor condition had an effect on the carbonate-to-phosphate ratio (Fig. 6D-F).

Finally, statistical analysis of the distribution of phosphate-to-collagen and carbonate-to-phosphate ratios along the antero-posterior axis of the ATE showed neither an effect of region nor an effect of condition on either ratio (data not shown).

4. Discussion

The first aim of this study was to demonstrate, by microindentation testing, a gradient of micromechanical properties along the longitudinal axis of the mineralized part of the healthy ATE. Our results show that the elastic modulus gradually increased along the mineralized part of the ATE from the tidemark to the subchondral bone, rising from 6.97 GPa (±1.03) to 12.88 GPa (±1.70) respectively. Thus, the enthesis becomes more rigid as it approaches the bone, which contributes to a gradual transition of mechanical properties from fibrocartilage to bone. Regarding hardness, our results show a trend towards gradual increase from the tidemark to the subchondral bone. Hardness captures a material's ability to withstand deformation; accordingly, our results show that the CFc of the enthesis increasingly hardens as it approaches the bone. Our results confirm findings from microindentation testing on other calcified cartilage and bone. Roseren et al. (2022) reported the same range of elastic moduli and hardness values in regenerating bone calluses where calcified fibrocartilage was produced by endochondral ossification. Regarding bone, Gerbaix et al. (2017) reported an elastic
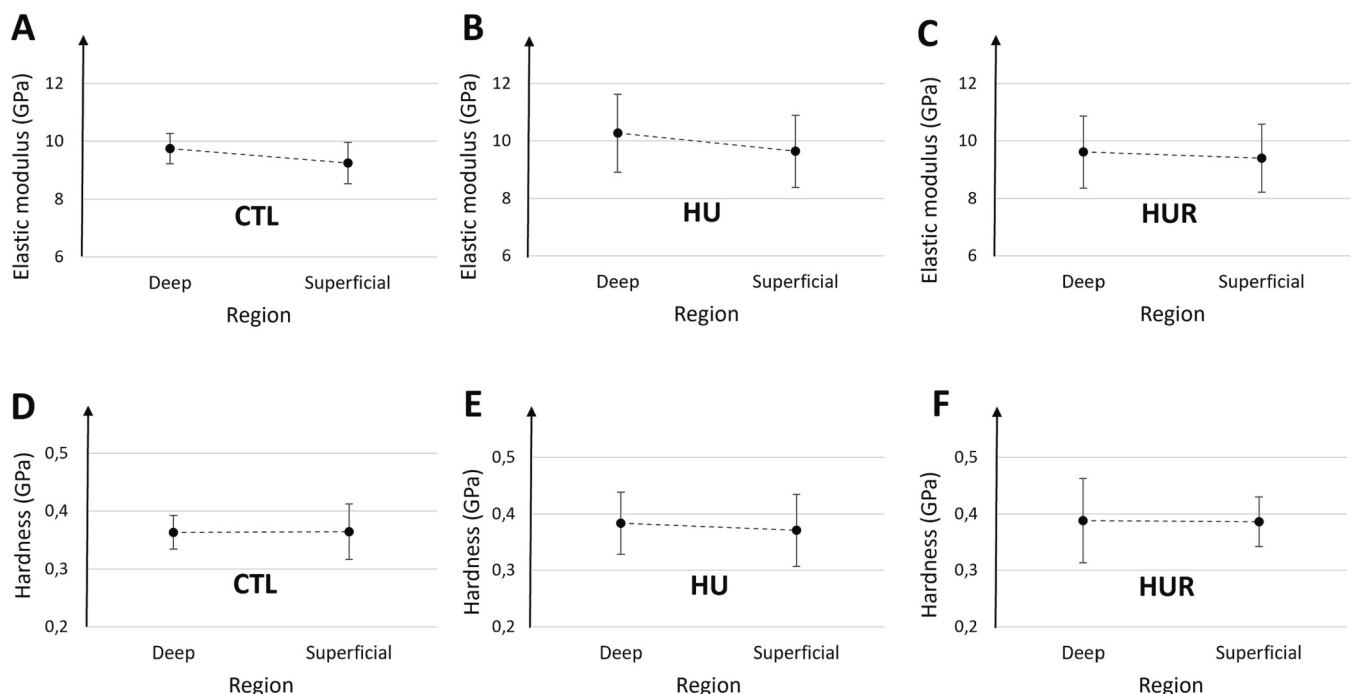

Fig. 5. Elastic modulus (A, B, C) and hardness (D, E, F) according to ATE region in CTL (A, D), HU (B, E) and HUR (C, F) conditions.
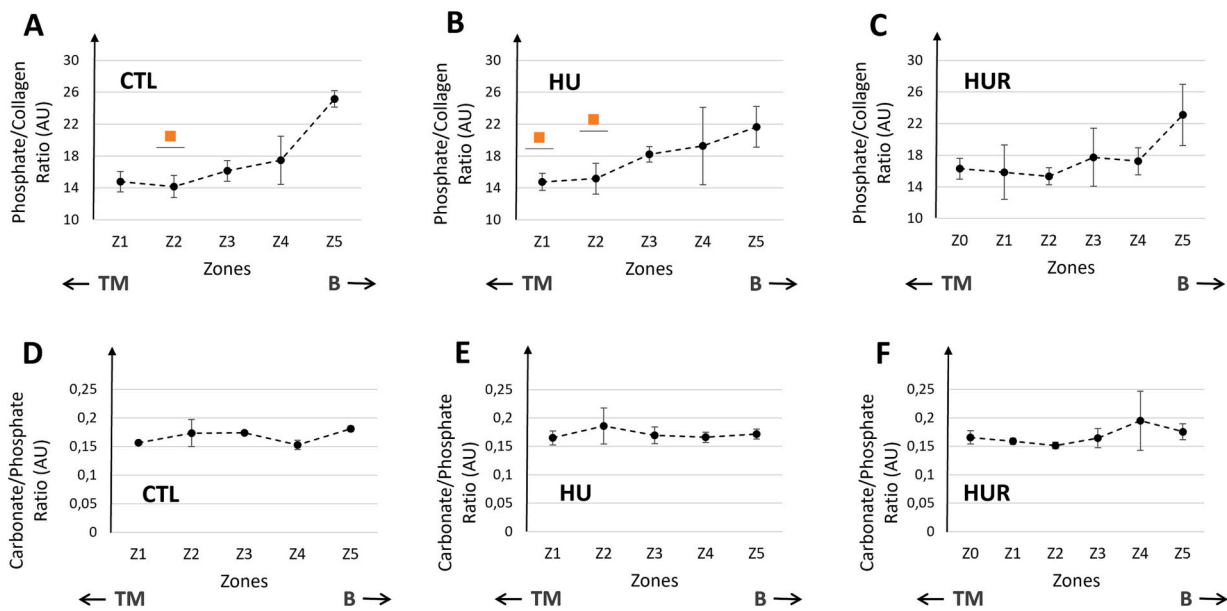
Fig. 6. Phosphate-to-Collagen ratio (A, B, C) and Carbonate-to-Phosphate ratio (D, E, F) according to ATE zone in CTL (A, D), HU (B, E), and HUR (C, F) conditions. TM: Tidemark. B: Bone. Orange square ■: significantly different from Z5 ($p < 0.05$).

modulus of about 13 GPa, and an average hardness of 0.6 GPa on trabecular bone in mice, comparable to our average elastic modulus of 12.88 GPa (±1,70) and average hardness of 0.465 GPa (±0,11) on healthy subchondral bone. Like these two studies, we performed our microindentation tests on resin-embedded samples previously fixed with paraformaldehyde. This sample-processing method has its limitations, leading to overestimation of the elastic modulus by about 15 % and of tissue hardness by 10 % (Zysset, 2009). In addition, we used the Oliver and Pharr (1992) method to estimate the material micromechanical parameters, which meant considering the CFc as an isotropic material, whereas an enthesis is anisotropic and has viscous properties. Nevertheless, this embedding technique and this calculation method are widely validated for mineralized tissues such as bone (Zysset, 2009).

Mineralization is known to have an impact on the micromechanical properties of biological tissue (Farlay et al., 2022; Gupta et al., 2005; Roseren et al., 2022; Zysset, 2009). Both elastic modulus and hardness depend on the degree of mineralization of the tissue (Farlay et al., 2022; Gupta et al., 2005; Roseren et al., 2022; Zysset, 2009). Another factor determining bone elastic modulus and hardness is crystallinity corresponding to the size and organization of apatite crystals (Farlay et al., 2022). Crystallinity depends in part on substitutions that occur in the crystal. Carbonate substitutions change the lattice of bone crystals, decreasing both the crystallinity and the size of crystals but increasing their solubility (Madupalli et al., 2017). Thus, we performed a Raman spectroscopy experiment to investigate the mineral-to-matrix ratio and the carbonation ratio along the mineralized part of the ATE.

We found that the carbonate-to-phosphate ratio representing the proportion of carbonate-substituted phosphate apatites was homogenous in the CFc of the ATE and did not differ from subchondral bone values. There was an average carbonate-to-phosphate ratio of 0.173 (±0.006) along the calcified part of enthesis, consistent with the findings of Deymier et al. (2020) and Schwartz et al. (2013) assessing the carbonate-to-phosphate ratio respectively on the calcaneus and on the supraspinatus developing enthesis in mice by Raman spectroscopy. Since the carbonate-to-phosphate ratio did not differ according to zone of measurement, we can reject the hypothesis that the gradient of the micromechanical properties we observed along the longitudinal axis of the ATE is related to carbonate-substituted phosphate apatites.

Analysis of the Raman spectra revealed that, unlike the carbonate-to-phosphate ratio, the phosphate-to-collagen ratio representing the

proportion of mineral within the extracellular matrix increased by >70 % from the tidemark to the subchondral bone. Statistically, however, probably due to a low number of samples and high standard deviations, only one zone of the CFc (Z2) differed significantly from the bone. It has long been established that fibrocartilaginous entheses are mineralized progressively between the mineralization front and the subchondral bone. A gradient in mineralization was demonstrated at the supraspinatus enthesis by Wopenka et al. (2008) and Genin et al. (2009) in mature rats and by Schwartz et al. (2013) in developing mice, using Raman spectroscopy. Deymier et al. (2017) also described a gradient in calcium content at this same enthesis in mature mice, using X-ray energy dispersive spectroscopy. However, very recently, using quantitative backscattered electron imaging, Tits et al. (2023) did not detect any gradient in mineral content at the rat Achilles tendon enthesis. In addition, using nanoindentation, the latter study reported no gradient in material properties within CFc except for a very small region of about 15 μm in width at the mineralization front. These observations are somewhat at odds with our results. The way in which measurement locations were determined cannot explain the divergences between the two studies' findings. Indeed, when we plotted our data as a function of the shortest distance from the tidemark according to the Tits et al. (2023) study, the gradient we observed by plotting our data by zone, was also present. The spatial organization of the osteochondral interface could rather explain the two studies' differing observations. Tits et al. (2023) reported isolated bone "islands" fully encircled by mFC several tens of micrometers away from the interface. This would support the hypothesis that the interdigitations between calcified fibrocartilage and subchondral bone in the rat Achilles tendon enthesis are not all oriented along the main axis of force transmission. We have never observed these islands in calcified fibrocartilage of the mouse Achilles tendon enthesis. Thus, in contrast to the rat, the interdigitations between mineralized fibrocartilage and subchondral bone appear to be less complex and oriented along the main axis of force transmission.

In our study, we observed that the changes in phosphate-to-collagen ratio along the mineralized part of the enthesis were correlated with changes in elastic modulus and hardness along the longitudinal axis of the ATE. Although we did not perform indentation and Raman spectroscopy on the same animals, we hypothesize with reasonable confidence that the gradient in mechanical properties we demonstrated through microindentation is in part explained by the observed

mineralization gradient in the healthy ATE. This assumption is consistent with a recent study that found, on cortical and trabecular bone, a positive correlation between elastic modulus, hardness, and phosphate-to-collagen ratio using indentation and Raman techniques (Farlay et al., 2022). However, other factors could also explain the ATE micromechanical properties we observed. In mineralized tissues, it has been suggested and/or demonstrated that elastic modulus and hardness depend on the maturity and orientation of apatite crystals, as well as on the composition, maturity, and organization of collagen fibers, and lastly on the non-collagenous matrix such as proteoglycans (Farlay et al., 2022; Zysset, 2009; Gupta et al., 2005; Hao et al., 2022). These parameters were not investigated in the present study. Future studies should focus on their potential influence on the mechanical properties gradient of the tendon enthesis.

Our second objective was to investigate the impact of a chronic variation in mechanical load applied to the ATE. A few studies have addressed the mechanical response of entheses to unloading at the macroscale (Matsumoto et al., 2003; Deymier et al., 2019; Deymier et al., 2020; Abraham et al., n.d.; Golman et al., 2021), but none at the microscale. Our study shows that a 14-day unloading period induced by hindlimb suspension, commonly used to simulate weightlessness in rodents, did not affect the gradient of micromechanical properties along the longitudinal axis of the mineralized part of the ATE. These results are consistent with our recent investigation (Camy et al., 2022) of the structural remodeling of the ATE, using the same animal model. In the latter study, CFc appeared to be very little affected by 14 days of unloading, with no change observed in fibrocartilage surface area, coll II expression, or collagen fiber organization, nor any sign of resorption at the osteochondral interface. The present Raman spectroscopy experiment provides additional evidence of a limited biological response to a short period of simulated microgravity, with neither the phosphate-to-collagen ratio nor the carbonate-to-phosphate ratio of HU animals differing from those of CTL animals. Taken together, our two studies demonstrate that, in contrast to the significant structural remodeling of the enthesis described for uncalcified fibrocartilage (Järvinen et al., 1999; Camy et al., 2022), a short period of mechanical unloading does not alter the micromechanical properties of the CFc of the ATE. Any biological changes in the CFc are therefore minor. Similar findings were reported in real microgravity conditions for the supraspinatus tendon enthesis (Deymier et al., 2020). Thus, it appears that the amplitude and duration of unloading need to be greater to induce CFc remodeling. Indeed, three weeks of botox-induced supraspinatus muscle paralysis impaired the mineral content of the developing and mature supraspinatus enthesis (Schwartz et al., 2013; Deymier et al., 2019).

As the subchondral bone is considered an integral part of the enthesis, we also assessed its hardness and elastic modulus. The values obtained for the HU animals did not differ from those of the CTL animals. Nor was there any difference between the two groups regarding phosphate-to-collagen and carbonate-to-phosphate ratios. The adverse effects of the microgravity environment on weight-bearing bones are widely documented (Bloomfield et al., 2016; Lang et al., 2017; Vico and Hargens, 2018). Although simulated and real microgravity conditions lead to losses in bone mass and bone mineral density (Roffino et al., 2021), bone density changes seem to occur after spaceflight longer than 28 days (Stavnichuk et al., 2020). For example, Deymier et al. (2020) reported no effect on the calcaneus phosphate-to-collagen ratio after 15 days of spaceflight. Our results are in line with this observation. Similarly, Gerbaix et al. (2017) showed that the mineral characteristics of the mouse femur (BMD, crystallinity index, mineralization index, mineral maturity, and carbonation) were preserved during a 1-month spaceflight. However, contrary to our results, these latter authors found a decrease in both elastic modulus and hardness. The longer duration of the flight, together with the constraints of the real microgravity environment, could explain this difference.

Finally, we investigated the effects of 6 days of reloading after HU on the CFc of the enthesis and on the subchondral bone. Our results show

that the CFc of the HUR ATE tended to lose its gradient of micromechanical properties along the longitudinal axis of the enthesis. Unlike the CTL and HU animals, the HUR animals showed no significant differences in elastic modulus among the four zones within the CFc. The HUR group's loss of elastic modulus gradient was due to a decreased value near the CFc-bone interface, where the elastic modulus was statistically lower than CTL samples. We observed the same trend with hardness, which was homogeneous in the CFc regardless of the zone assessed. This observation is not surprising, since it has been demonstrated that elastic modulus and hardness are linearly correlated (Evans et al., 1990).

Impairment of the micromechanical properties of the HUR enthesis appeared to be independent of carbonate-to-phosphate ratios, with similar values obtained regardless of experimental condition. We speculate that the standardization of micromechanical properties within the enthesis CFc could stem from homogenization of the degree of mineralization. Unfortunately, we cannot validate this hypothesis with certainty, since our Raman spectroscopy yielded few statistically significant differences. The degree of mineralization appeared to be altered in the zone close to the osteochondral interface (Z4), suggesting decreased mineralization compared to the CTL and HU groups. Since no resorption activity was found at the osteochondral interface of the ATE under the same experimental conditions (Camy et al., 2022), the trend towards reduced mineralization could stem from an increase in mineral degradation unrelated to chondroclastic activity. An impaired mineralization process in this highly mineralized zone could also account for the decrease. The mineralization process is known to be modified with a return to normal mechanical stress. A progression of the mineralization front towards the tendon has been reported in the ATE in response to 6 days of reloading (Camy et al., 2022). The present work characterized this newly-mineralized part of the CFc (Z0), where we found highly variable hardness. While Z0's average hardness did not differ from that of the subchondral bone, its hardness values were above those of all the other CFc zones. Since hardness is highly dependent on mineral characteristics, the observed variability may reflect either different degrees of crystallinity and varying mineral properties (Wittig et al., 2019; Grünewald et al., 2023) or a different distribution of mineral fraction (intra vs extrafibrillar) (Grünewald et al., 2020; Macías-Sánchez et al., 2022) rather than distinct changes in the degree of mineralization. Here, Z0 did not show differences in degree of mineralization and carbonation from the other CFc zones. It could be argued that the stimulation of the mineralization process during reloading occurs exclusively in Z0. The study of Kannus et al. (1996), which explored the expression of osteocalcin in the rat proximal patellar enthesis in response to reloading, supports this hypothesis. These authors reported increased osteocalcin expression throughout the CFc in reloaded rats, suggesting that the mineralization process may be initiated throughout the CFc. However, the process might be negatively impacted locally near the osteochondral interface, which would explain a leveling of both degrees of mineralization and micromechanical properties. Proteoglycans, macromolecules of the non-collagenous matrix known to have a rapid turnover (Cook et al., 2016), could play a role in the early changes we observed 6 days after reloading. On bone, SLRPs negatively regulate the maturity and growth of apatite crystals (Farlay et al., 2022; Hao et al., 2022; Waddington et al., 2003). Interestingly, it has been demonstrated that the expression of decorin, which belongs to the SLRP family, is not uniform within entheseal fibrocartilage. In healthy entheses, it is very strongly expressed both near the osteochondral junction and in the uncalcified ficrocartilage (Waggett et al., 1998), probably to prevent progression of ossification fronts at the tidemark and at the osteochondral junction. Thus, a change in decorin distribution in the CFc entailing excessive overexpression at the osteochondral junction could lead to defective mineralization. We could not investigate the proteoglycans by Raman spectroscopy because proteoglycans spectra are complex and their signal partly overlaps with other tissue components (Ellis et al., 2009; Bergholt et al., 2019). Furthermore, we were using toluidine blue stain

to determine the location of the indents, and this dye did not allow us to distinguish the different types of proteoglycans. Mineralization along the CFc is not the only parameter that determines the micromechanical properties of the enthesis; the collagenous matrix also influences the micromechanical properties of mineralized tissues (Farlay et al., 2022; Hao et al., 2022). Collagen type, orientation, and maturation have an impact on both their elastic modulus and their hardness (Farlay et al., 2022; Gupta et al., 2005; Roseren et al., 2022; Zysset, 2009). Further work is needed to clarify whether these factors are indeed responsible for the mechanical response along the longitudinal axis of the ATE at the microscale.

It is commonly recognized in the literature that fibrocartilaginous entheses have a gradient of mechanical properties along the longitudinal axis of force transmission that prevent injury by dissipating mechanical stress at the interface (Schwartz et al., 2012; Smith et al., 2012). Our study demonstrates that this gradient exists locally, in the mineralized part of the Achilles enthesis. It also shows that, contrary to a short period of unloading, an early return to normal mechanical load can cause a loss of this micromechanical properties gradient. Given its presumed function, the loss of gradient shown in the mineralized portion of the reloaded enthesis could have impaired the tensile resistance of the interface. However, we previously showed, under the same experimental conditions, that the ATE's ability to withstand tensile stress was not adversely impacted by reloading (Camy et al., 2022). It should be remembered that, due to methodological limitations, we could only characterize the gradient in the mineralized part of the enthesis. Thus, the adverse effects of the return to normal load on the CFc mineral gradient may have been offset by the increase in both proteoglycan content and degree of collagen fiber crimp, helping perhaps to dissipate the mechanical stress. Confirming this hypothesis will require further research, including the development of a method of characterizing the enthesis' local micromechanical properties in the non-calcified fibrocartilage.

In addition to the distribution of the micromechanical properties along the longitudinal axis (zone effect), we were also interested in the distribution of these properties along the antero-posterior axis (region effect). In humans, it has been demonstrated that the deep and the superficial regions of a "healthy" Achilles tendon insertion in its tendinous part do not undergo the same strains during dorsiflexion movements (Lyman et al., 2004; Chimenti et al., 2016). This difference in strains may reflect local variation in the tissue's mechanical properties. But it could also reflect local variation in the stress applied to the tissue, as suggested by McGonagle et al. (2008). These authors hypothesized that force transmission occurred mainly on the superficial part of the enthesis (McGonagle et al., 2008), leading us to explore whether there was a non-homogeneous distribution of mechanical properties in the CFc along the antero-posterior axis. Our results show no difference in hardness between superficial and deep regions in the CFc but a difference in elastic modulus. Elastic moduli were statistically lower in the superficial region of the CFc than in the deep region, regardless of condition. The difference we found was comparatively modest and, since this difference was not found within each group, it cannot confidently be concluded that it has a biological significance. In an analogous study in mice, elevated strain magnitudes were observed both in the superficial and the deep (closest to the bone) regions of the Achilles tendon insertion (Mora et al., 2022). In addition, the fact that neither unloading nor reloading had any effect on the distribution of hardness and elastic modulus along the antero-posterior axis of the enthesis, consistent with Mora et al. (2022), actually supports the idea that, contrary to humans, force transmission at the mouse enthesis is uniform at all depths of the ATE.

5. Conclusion

This characterization of the micromechanical properties of the ATE and its response to chronic changes in mechanical load provides valuable data not only for tissue bioengineering, but also for musculoskeletal

clinical studies and microgravity studies focusing on long-term space travel by astronauts. The ATE, like the rotator cuff tendon enthesis and the patellar tendon enthesis, is a common site of injuries (Derwin et al., 2018; Loukopoulou et al., 2022). Tendon rupture may occur at the tendon-to-bone insertion of a healthy tendon after acute trauma, or be due to a defective tendon weakened by an enthesopathy (Derwin et al., 2018). Complete tendon rupture at the bone-tendon interface requires surgical reattachment of the soft tendon directly to the hard bone. Unfortunately, healing occurs through the formation of disorganized scar tissue rather than in an ordered fibrocartilaginous transition, reducing the mechanical properties of the surgically-treated enthesis compared to the native interface (Derwin et al., 2018; Loukopoulou et al., 2022; Lei et al., 2021). This results in poor clinical outcomes and high failure rates (Tits and Ruffoni, 2021; Lei et al., 2021), which highlights the need for effective strategies for regenerating injured entheses. However, limited understanding of tissue boundaries, gradients, and structural relationships is hampering the development of novel therapeutic strategies for enthesis regeneration and reducing their direct clinical applicability (Loukopoulou et al., 2022). In this context, our study contributes to a better understanding of the enthesis structure, a prerequisite for the biomimetic strategies that are needed to achieve functional enthesis repair.

CRediT authorship contribution statement

Claire Camy: Writing – review & editing, Writing – original draft, Methodology, Investigation, Data curation, Conceptualization. **Tilman Grünewald:** Writing – review & editing, Validation, Methodology, Data curation. **Edouard Lamy:** Writing – review & editing, Validation, Methodology, Data curation. **Flavy Roseren:** Writing – review & editing, Validation, Methodology, Data curation. **Mathieu Caumes:** Writing – review & editing, Methodology, Data curation. **Théo Fovet:** Writing – review & editing, Methodology. **Thomas Brioche:** Writing – review & editing, Methodology. **Cecile Genovesio:** Writing – review & editing, Methodology. **Angèle Chopard:** Writing – review & editing, Validation, Supervision, Conceptualization. **Martine Pithioux:** Writing – review & editing, Visualization, Validation, Supervision, Methodology, Conceptualization. **Sandrine Roffino:** Writing – review & editing, Writing – original draft, Visualization, Validation, Supervision, Methodology, Investigation, Data curation, Conceptualization.

Declaration of competing interest

All the authors declare that they have no known competing financial interests or personal relationships that could have appeared to influence the work reported in this paper.

Data availability

Data will be made available on request.

References

Abraham, A. C., Fang, F., Golman, M., Oikonomou, P., & Thomopoulos, S. (s.d.). The role of loading in murine models of rotator cuff disease. J. Orthop. Res., n/a(n/a). https://doi.org/10.1002/jor.25113.

Amblard, D., Lafage-Proust, M.-H., Laib, A., Thomas, T., Rüegsegger, P., Alexandre, C., Vico, L., 2003. Tail suspension induces bone loss in skeletally mature mice in the C57BL/6J strain but not in the C3H/HeJ strain. J. Bone Miner. Res. 18 (3), 561–569. https://doi.org/10.1359/jbmr.2003.18.3.561.

Benjamin, M., McGonagle, D., 2001. The anatomical basis for disease localisation in seronegative spondyloarthropathy at entheses and related sites. J. Anat. 199 (Pt 5), 503–526. https://doi.org/10.1046/j.1469-7580.2001.19950503.x.

Bergholt, M.S., Serio, A., Albro, M.B., 2019. Raman spectroscopy: guiding light for the extracellular matrix. Front. Bioeng. Biotechnol. 7, 303. https://doi.org/10.3389/fbioe.2019.00303.

Bloomfield, S.A., Martinez, D.A., Boudreaux, R.D., Mantri, A.V., 2016. Microgravity stress: bone and connective tissue. Compr. Physiol. 6 (2), 2 https://doi.org/10.1002/cphy.c130027.

Bunker, D.L.J., Ilie, V., Ilie, V., Nicklin, S., 2014. Tendon to Bone Healing and Its Implications for Surgery, 8.

Camy, C., Brioche, T., Senni, K., Bertaud, A., Genovesio, C., Lamy, E., Fovet, T., Chopard, A., Pithioux, M., Roffino, S., 2022. Effects of hindlimb unloading and subsequent reloading on the structure and mechanical properties of Achilles tendon-to-bone attachment. FASEB J. 36 (10), e22548 https://doi.org/10.1096/fj.202200713R.

Chimenti, R.L., Flemister, A.S., Ketz, J., Bucklin, M., Buckley, M.R., Richards, M.S., 2016. Ultrasound strain mapping of Achilles tendon compressive strain patterns during dorsiflexion. J. Biomech. 49 (1), 39–44. https://doi.org/10.1016/j.jbiomech.2015.11.008.

Cook, J.L., Rio, E., Purdam, C.R., Docking, S.I., 2016. Revisiting the continuum model of tendon pathology: what is its merit in clinical practice and research? Br. J. Sports Med. 50 (19), 1187–1191. https://doi.org/10.1136/bjsports-2015-095422.

Crawford-Manning, F., Vardaki, M.Z., Green, E., Meakin, J.R., Vergari, C., Stone, N., Peter Winlove, C., 2021. Multiphoton imaging and Raman spectroscopy of the bovine vertebral endplate. Analyst 146 (13), 4242–4253. https://doi.org/10.1039/D1AN00702E.

Cury, D.P., Dias, F.J., Miglino, M.A., Watanabe, I., 2016. Structural and ultrastructural characteristics of bone-tendon junction of the calcaneal tendon of adult and elderly Wistar rats. PLoS One 11 (4), 4. https://doi.org/10.1371/journal.pone.0153568.

Curzi, D., 2016. Ultrastructural study of myotendinous junction plasticity: from disuse to exercise. Sport Sci. Health 12 (3), 279–286. https://doi.org/10.1007/s11332-016-0301-1.

Das Gupta, S., Finnilä, M.A.J., Karhula, S.S., Kauppinen, S., Joukainen, A., Kröger, H., Korhonen, R.K., Thambyah, A., Rieppo, L., Saarakkala, S., 2020. Raman microspectroscopic analysis of the tissue-specific composition of the human osteochondral junction in osteoarthritis: a pilot study. Acta Biomater. 106, 145–155. https://doi.org/10.1016/j.actbio.2020.02.020.

Derwin, K.A., Galatz, L.M., Ratcliffe, A., Thomopoulos, S., 2018. Enthesis repair: challenges and opportunities for effective tendon-to-bone healing. J. Bone Joint Surg. Am. 100 (16), e109 https://doi.org/10.2106/JBJS.18.00200.

Deymier, A.C., An, Y., Boyle, J.J., Schwartz, A.G., Birman, V., Genin, G.M., Thomopoulos, S., Barber, A.H., 2017. Micro-mechanical properties of the tendon-to-bone attachment. Acta Biomater. 56, 25–35. https://doi.org/10.1016/j.actbio.2017.01.037.

Deymier, A.C., Schwartz, A.G., Cai, Z., Daulton, T.L., Pasteris, J.D., Genin, G.M., Thomopoulos, S., 2019. The multiscale structural and mechanical effects of mouse supraspinatus muscle unloading on the mature enthesis. Acta Biomater. 83, 302–313. https://doi.org/10.1016/j.actbio.2018.10.024.

Deymier, A.C., Schwartz, A.G., Lim, C., Wingender, B., Kotiya, A., Shen, H., Silva, M.J., Thomopoulos, S., 2020. Multiscale effects of spaceflight on murine tendon and bone. Bone 131, 115152. https://doi.org/10.1016/j.bone.2019.115152.

Ellis, R., Green, E., Winlove, C.P., 2009. Structural analysis of glycosaminoglycans and proteoglycans by means of Raman microspectrometry. Connect. Tissue Res. 50 (1), 29–36. https://doi.org/10.1080/03008200802398422.

Evans, G.P., Behiri, J.C., Currey, J.D., Bonfield, W., 1990. Microhardness and Young's modulus in cortical bone exhibiting a wide range of mineral volume fractions, and in a bone analogue. J. Mater. Sci. Mater. Med. 1 (1), 38–43. https://doi.org/10.1007/BF00705352.

Farlay, D., Falgayrac, G., Ponçon, C., Rizzo, S., Cortet, B., Chapurlat, R., Penel, G., Badoud, I., Ammann, P., Boivin, G., 2022. Material and nanomechanical properties of bone structural units of cortical and trabecular iliac bone tissues from untreated postmenopausal osteoporotic women. Bone Rep. 17, 101623 https://doi.org/10.1016/j.bonr.2022.101623.

Friese, N., Gierschner, M.B., Schadzek, P., Roger, Y., Hoffmann, A., 2020. Regeneration of damaged tendon-bone junctions (Entheses)—TAK1 as a potential node factor. Int. J. Mol. Sci. 21 (15), 15 https://doi.org/10.3390/ijms21155177.

Frizziero, A., Fini, M., Salamanna, F., Veicsteinas, A., Maffulli, N., Marini, M., 2011. Effect of training and sudden detraining on the patellar tendon and its enthesis in rats. BMC Musculoskelet. Disord. 12, 20. https://doi.org/10.1186/1471-2474-12-20.

Genin, G.M., Kent, A., Birman, V., Wopenka, B., Pasteris, J.D., Marquez, P.J., Thomopoulos, S., 2009. Functional grading of mineral and collagen in the attachment of tendon to bone. Biophys. J. 97 (4), 976–985. https://doi.org/10.1016/j.bpj.2009.05.043.

Gerbaix, M., Gnyubkin, V., Farlay, D., Olivier, C., Ammann, P., Courbon, G., Laroche, N., Genthial, R., Follet, H., Peyrin, F., Shenkman, B., Gauquelin-Koch, G., Vico, L., 2017. One-month spaceflight compromises the bone microstructure, tissue-level mechanical properties, osteocyte survival and lacunae volume in mature mice skeletons. Sci. Rep. 7 (1), 2659. https://doi.org/10.1038/s41598-017-03014-2.

Golman, M., Abraham, A.C., Kurtaliaj, I., Marshall, B.P., Hu, Y.J., Schwartz, A.G., Guo, X. E., Birman, V., Thurner, P.J., Genin, G.M., Thomopoulos, S., 2021. Toughening mechanisms for the attachment of architectured materials: the mechanics of the tendon enthesis. Sci. Adv. 7 (48), eabi5584 https://doi.org/10.1126/sciadv.abi5584.

Grünewald, T.A., Liebi, M., Wittig, N.K., Johannes, A., Sikjaer, T., Rejnmark, L., Gao, Z., Rosenthal, M., Guizar-Sicairos, M., Birkedal, H., Burghammer, M., 2020. Mapping the 3D orientation of nanocrystals and nanostructures in human bone: indications of novel structural features. Sci. Adv. 6 (24), eaba4171 https://doi.org/10.1126/sciadv.aba4171.

Grünewald, T.A., Johannes, A., Wittig, N.K., Palle, J., Rack, A., Burghammer, M., Birkedal, H., 2023. Bone mineral properties and 3D orientation of human lamellar bone around cement lines and the Haversian system. IUCrJ 10 (2), 2. https://doi.org/10.1107/S2052252523000866.

Gupta, H.S., Schratter, S., Tesch, W., Roschger, P., Berzlanovich, A., Schoeberl, T., Klaushofer, K., Fratzl, P., 2005. Two different correlations between nanoindentation modulus and mineral content in the bone–cartilage interface. J. Struct. Biol. 149 (2), 138–148. https://doi.org/10.1016/j.jsb.2004.10.010.

Hao, J.-X., Shen, M.-J., Wang, C.-Y., Wei, J.-H., Wan, Q.-Q., Zhu, Y.-F., Ye, T., Luo, M.-L., Qin, W.-P., Li, Y.-T., Jiao, K., Zhao, B., Niu, L.-N., 2022. Regulation of biomineralization by proteoglycans: from mechanisms to application. Carbohydr. Polym. 294, 119773 https://doi.org/10.1016/j.carbpol.2022.119773.

Hu, K., Radhakrishnan, P., Patel, R.V., Mao, J.J., 2001. Regional structural and viscoelastic properties of fibrocartilage upon dynamic nanoindentation of the articular condyle. J. Struct. Biol. 136 (1), 46–52. https://doi.org/10.1006/jsbi.2001.4417.

Järvinen, T.A., Jozsa, L., Kannus, P., Järvinen, T.L., Kvist, M., Hurme, T., Isola, J., Kalimo, H., Järvinen, M., 1999. Mechanical loading regulates tenascin-C expression in the osteotendinous junction. J. Cell Sci. 112 (Pt 18), 3157–3166.

Kannus, P., Jozsa, L., Kvist, M., Järvinen, T.L., Maunu, V.M., Hurme, T., Järvinen, M., 1996. Expression of osteocalcin in the patella of experimentally immobilized and remobilized rats. J. Bone Miner. Res. Off. J. Am. Soc. Bone Miner. Res. 11 (1), 79–87. https://doi.org/10.1002/jbmr.5650110112.

Kazanci, M., Roschger, P., Paschalis, E.P., Klaushofer, K., Fratzl, P., Dec 2006. Bone osteonal tissues by Raman spectral mapping: orientation-composition. J. Struct. Biol. 156 (3), 489–496. https://doi.org/10.1016/j.jsb.2006.06.011 (Epub 2006 Jul 16. PMID: 16931054).

Kumagai, J., Sarkar, K., Uthhoff, H.K., Okawara, Y., Ooshima, A., 1994. Immunohistochemical distribution of type I, II and III collagens in the rabbit supraspinatus tendon insertion. J. Anat. 185 (Pt 2), 279–284.

Lang, T., Van Loon, J.J.W.A., Bloomfield, S., Vico, L., Chopard, A., Rittweger, J., Kyparos, A., Blottner, D., Vuori, I., Gerzer, R., Cavanagh, P.R., 2017. Towards human exploration of space: the THESEUS review series on muscle and bone research priorities. Npj Microgravity 3 (1), 1. https://doi.org/10.1038/s41526-017-0013-0.

Lei, T., Zhang, T., Ju, W., Chen, X., Heng, B.C., Shen, W., Yin, Z., 2021. Biomimetic strategies for tendon/ligament-to-bone interface regeneration. Bioactive Mater. 6 (8), 2491–2510. https://doi.org/10.1016/j.bioactmat.2021.01.022.

Liu, Y., Birman, V., Chen, C., Thomopoulos, S., Genin, G.M., 2011. Mechanisms of bimaterial attachment at the interface of tendon to bone. J. Eng. Mater. Technol. 133 (1) https://doi.org/10.1115/1.4002641.

Loukopoulou, C., Mortimer, J.W., Paxton, J.Z., 2022. Making connections: using anatomy to guide tissue engineering approaches at the enthesis. Eur. Cell. Mater. 43, 162–178. https://doi.org/10.22203/eCM.v043a14.

Lyman, J., Weinhold, P.S., Almekinders, L.C., 2004. Strain behavior of the distal Achilles tendon: implications for insertional Achilles tendinopathy. Am. J. Sports Med. 32 (2), 457–461. https://doi.org/10.1177/0095399703258621.

Macías-Sánchez, E., Tarakina, N.V., Ivanov, D., Blouin, S., Berzlanovich, A.M., Fratzl, P., 2022. Spherulitic crystal growth drives mineral deposition patterns in collagen-based materials. Adv. Funct. Mater. 32 (31), 2200504 https://doi.org/10.1002/adfm.202200504.

Madupalli, H., Pavan, B., Tecklenburg, M.M.J., 2017. Carbonate substitution in the mineral component of bone: discriminating the structural changes, simultaneously imposed by carbonate in A and B sites of apatite. J. Solid State Chem. 255, 27–35. https://doi.org/10.1016/j.jssc.2017.07.025.

Mandair, G.S., Morris, M.D., 2015. Contributions of Raman spectroscopy to the understanding of bone strength. BoneKEy Rep. 4 https://doi.org/10.1038/bonekey.2014.115.

Matsumoto, F., Trudel, G., Uthhoff, H.K., Backman, D.S., 2003. Mechanical effects of immobilization on the Achilles' tendon. Arch. Phys. Med. Rehabil. 84 (5), 662–667. https://doi.org/10.1016/S0003-9993(02)04834-7.

Mazet, V., Carteret, C., Brie, D., Idier, J., Humbert, B., 2005. Background removal from spectra by designing and minimising a non-quadratic cost function. Chemom. Intell. Lab. Syst. 76 (2), 121–133. https://doi.org/10.1016/j.chemolab.2004.10.003.

McGonagle, D., Wakefield, R.J., Tan, A.L., D'Agostino, M.A., Toumi, H., Hayashi, K., Emery, P., Benjamin, M., 2008. Distinct topography of erosion and new bone

formation in achilles tendon enthesitis: implications for understanding the link between inflammation and bone formation in spondylarthritis. Arthritis Rheum. 58 (9), 2694–2699. https://doi.org/10.1002/art.23755.

Mora, K.E., Mlawer, S.J., Bae, A.J., Richards, M.S., Loiselle, A.E., Buckley, M.R., 2022. Ultrasound strain mapping of the mouse Achilles tendon during passive dorsiflexion. J. Biomech. 132, 110920 https://doi.org/10.1016/j.jbiomech.2021.110920.

Morey-Holton, E.R., Globus, R.K., 1998. Hindlimb unloading of growing rats: a model for predicting skeletal changes during space flight. Bone 22 (5 Suppl), 83S–88S. https://doi.org/10.1016/s8756-3282(98)00019-2.

Moriggl, B., Kumai, T., Milz, S., Benjamin, M., 2003. The structure and histopathology of the « enthesis organ » at the navicular insertion of the tendon of tibialis posterior. J. Rheumatol. 30 (3), 3.

Mutsuzaki, H., Nakajima, H., Wadano, Y., Takahashi, H., Sakane, M., 2015. Influence of mechanical unloading on histological changes of the patellar tendon insertion in rabbits. Knee 22 (6), 6. https://doi.org/10.1016/j.knee.2015.03.004.

Oliver, W.C., Pharr, G.M., 1992. An improved technique for determining hardness and elastic modulus using load and displacement sensing indentation experiments. J. Mater. Res. 7 (6), 1564–1583. https://doi.org/10.1557/JMR.1992.1564.

Ralphs, J.R., Tyers, R.N., Benjamin, M., 1992. Development of functionally distinct fibrocartilages at two sites in the quadriceps tendon of the rat: the suprapatella and the attachment to the patella. Anat. Embryol. 185 (2), 2.

Roffino, S., Camy, C., Foucault-Bertaud, A., Lamy, E., Pithioux, M., Chopard, A., 2021. Negative impact of disuse and unloading on tendon enthesis structure and function. Life Sci. Space Res. https://doi.org/10.1016/j.lssr.2021.03.001.

Roseren, F., Roffino, S., Pithioux, M., 2022. Mechanical characterization at the microscale of mineralized bone callus after bone lengthening. Materials (Basel, Switzerland) 15 (18), 6207. https://doi.org/10.3390/ma15186207.

Sartori, J., Stark, H., 2020. Tracking tendon fibers to their insertion – a 3D analysis of the Achilles tendon enthesis in mice. Acta Biomater., S1742706120302622 https://doi.org/10.1016/j.actbio.2020.05.001.

Schwartz, A.G., Pasteris, J.D., Genin, G.M., Daulton, T.L., Thomopoulos, S., 2012. Mineral distributions at the developing tendon enthesis. PLoS One 7 (11), e48630. https://doi.org/10.1371/journal.pone.0048630.

Schwartz, A.G., Lipner, J.H., Pasteris, J.D., Genin, G.M., Thomopoulos, S., 2013. Muscle loading is necessary for the formation of a functional tendon enthesis. Bone 55 (1), 1. https://doi.org/10.1016/j.bone.2013.03.010.

Shaw, H.M., Benjamin, M., 2007. Structure–function relationships of entheses in relation to mechanical load and exercise. Scand. J. Med. Sci. Sports 17 (4), 303–315. https://doi.org/10.1111/j.1600-0838.2007.00689.x.

Smith, L., Xia, Y., Galatz, L.M., Genin, G.M., Thomopoulos, S., 2012. Tissue engineering strategies for the tendon/ligament-to-bone insertion. Connect. Tissue Res. 53 (2), 95–105. https://doi.org/10.3109/03008207.2011.650804.

Stavnichuk, M., Mikolajewicz, N., Corlett, T., Morris, M., Komarova, S.V., 2020. A systematic review and meta-analysis of bone loss in space travelers. NPJ Microgravity 6, 13. https://doi.org/10.1038/s41526-020-0103-2.

Thomopoulos, S., Williams, G.R., Gimbel, J.A., Favata, M., Soslowsky, L.J., 2003. Variation of biomechanical, structural, and compositional properties along the tendon to bone insertion site. J. Orthop. Res.: Off. Publ. Orthop. Res. Soc. 21 (3), 3 https://doi.org/10.1016/S0736-0266(03)00057-3.

Tits, A., Ruffoni, D., 2021. Joining soft tissues to bone: insights from modeling and simulations. Bone Rep. 14, 100742 https://doi.org/10.1016/j.bonr.2020.100742.

Tits, A., Plougonven, E., Blouin, S., Hartmann, M.A., Kaux, J.-F., Drion, P., Fernandez, J., van Lenthe, G.H., Ruffoni, D., 2021. Local anisotropy in mineralized fibrocartilage and subchondral bone beneath the tendon-bone interface. Sci. Rep. 11 (1), 16534 https://doi.org/10.1038/s41598-021-95917-4.

Tits, A., Blouin, S., Rummler, M., Kaux, J.F., Drion, P., van Lenthe, G.H., Weinkamer, R., Hartmann, M.A., Ruffoni, D., Aug 2023. Structural and functional heterogeneity of mineralized fibrocartilage at the Achilles tendon-bone insertion. Acta Biomater. 166, 409–418. https://doi.org/10.1016/j.actbio.2023.04.018 (Epub 2023 Apr 22. PMID: 37088163).

Turner, C., Burr, D., 2001. Experimental techniques for bone mechanics. In: Cowin, S. (Ed.), Bone Mechanics Handbook, Second edition. CRC Press, pp. 7-1–7-35. https://doi.org/10.1201/b14263-10.

Vico, L., Hargens, A., 2018. Skeletal changes during and after spaceflight. Nat. Rev. Rheumatol. 14 (4), 4 https://doi.org/10.1038/nrrheum.2018.37.

Waddington, R.J., Roberts, H.C., Sugars, R.V., Schönherr, E., 2003. Differential roles for small leucine-rich proteoglycans in bone formation. Eur. Cell. Mater. 6, 12–21. https://doi.org/10.22203/ecm.v006a02 (discussion 21).

Waggett, A.D., Ralphs, J.R., Kwan, A.P., Woodnutt, D., Benjamin, M., 1998. Characterization of collagens and proteoglycans at the insertion of the human Achilles tendon. Matrix Biol.: J. Int. Soc. Matrix Biol. 16 (8), 8.

Waghray, N., Jyothi, G.A., Imran, M., Yaseen, S., Chaudhary, U., 2015. Enthesis: a brief review. Apollo Med. 12 (1), 1 https://doi.org/10.1016/j.apme.2015.01.003.

Wittig, N.K., Palle, J., Østergaard, M., Frølich, S., Birkbak, M.E., Spiers, K.M., Garrevoet, J., Birkedal, H., 2019. Bone biomineral properties vary across human osteonal bone. ACS Nano 13 (11), 12949–12956. https://doi.org/10.1021/acsnano.9b05535.

Wopenka, B., Kent, A., Pasteris, J.D., Yoon, Y., Thomopoulos, S., 2008. The tendon-to-bone transition of the rotator cuff: a preliminary Raman spectroscopic study documenting the gradual mineralization across the insertion in rat tissue samples. Appl. Spectrosc. 62 (12), 1285–1294. https://doi.org/10.1366/000370208786822179.

Zelzer, E., Blitz, E., Killian, M.L., Thomopoulos, S., 2014. Tendon-to-bone attachment: from development to maturity. Birth Defects Res. C. Embryo Today 102 (1), 101–112. https://doi.org/10.1002/bdrc.21056.

Zhang, T., Li, S., Chen, Y., Xiao, H., Wang, L., Hu, J., Xu, D., Lu, H., 2022. Characterize the microstructure change after tendon enthesis injury using synchrotron radiation μCT. J. Orthop. Res. 40 (11), 2678–2687. https://doi.org/10.1002/jor.25289.

Zysset, P.K., 2009. Indentation of bone tissue: a short review. Osteoporos. Int. 20 (6), 1049–1055. https://doi.org/10.1007/s00198-009-0854-9.